Comparison of Regional Blood-Brain Transport Kinetics Between Glucose and Fluorodeoxyglucose

James L. Lear and Robert F. Ackerman

Nuclear Medicine Division, Department of Radiology, University of Colorado Health Sciences Center, Denver, Colorado; and Nuclear Medicine and Biophysics Division, Department of Radiological Sciences, UCLA School of Medicine, Los Angeles, California

The fluorodeoxyglucose (FDG) method for estimating regional cerebral glucose metabolic rate (LCMRglc) requires that a fixed relationship (the "lumped constant") exists between net FDG and glucose (GLC) extraction throughout the brain. In addition to the relative rate of metabolism between FDG and GLC, this assumed constant is affected by the relative rate of blood-to-brain FDG transport compared to that of glucose. However, little data is available regarding the regional stability of the FDG versus GLC transport-rate relationship. We therefore used high resolution, quantitative dual-tracer digital autoradiography to directly compare the blood-to-brain transport rate constants (K1) of radiolabeled GLC and FDG in normal and pharmacologically-stimulated rats. The rats were given 45 sec terminal intravenous infusions of a mixture of ^{18}F-FDG and ^{14}C-GLC. Autoradiograms of the brain representing the FDG and GLC tracer concentrations were produced, digitized, and converted into digital images of K1. We found that the global K1 values of FDG and GLC were not significantly different from each other. However, detailed analysis revealed that some structures in the normal animals, such as the hippocampus and cerebellum, had different quantitative patterns of FDG transport compared to GLC transport. Thus, our results indicate that the relationship between GLC and FDG transport is not uniform throughout the brain as has previously been assumed. This observation suggests that regional variations in the type and distribution of glucose transporters may exist and that the fluorodeoxyglucose "lumped constant" may vary somewhat among different brain regions.

J Nucl Med 1992; 33:1819–1824

Deoxyglucose (DG) and fluorodeoxyglucose (FDG) have been shown to generally behave as glucose analogs with respect to their transport from the blood into the brain and to their subsequent phosphorylation. This phenomenon is the basis for the widely used Sokoloff method (*1*) of quantification of local cerebral glucose metabolic rate (LCMRglc), in which a globally-applied "lumped constant" is used to convert the regional rates of DG- or FDG-derived radiolabel accumulation into values of LCMRglc. The DG and FDG methods thus assume that some fixed relationship between the net fluxes of DG or FDG and glucose exists throughout the brain. Because these net fluxes depend upon transport as well as metabolism, the relative rate of DG or FDG transport compared to that of glucose (GLC) and of DG or FDG phosphorylation compared to that of glucose must not vary regionally if a single "lumped constant" is to apply to the entire brain.

In fact, double tracer, FDG-GLC, studies have shown that in most normal animal structures, the cerebral accumulation rate of radiolabel derived from FDG in 30–45 min experiments is qualitatively similar to, and quantitatively related to, the distribution pattern of radiolabel derived from GLC in six to ten min experiments (*2*). However, in some regions such as the hippocampus, thalamus and cerebellum, the distribution patterns of FDG- and GLC-derived radiolabel differ (*2,3*). Also, activation causes other significant differences in patterns to occur, as the FDG-derived radiolabel accumulation can greatly exceed that of GLC in the activated regions (*4*).

These differences have been shown at least in part to be related to loss of GLC-derived radiolabel through production of radiolabeled CO_2 and lactate and the efflux of these compounds from the brain (*4,5*). However, the question arises as to whether these differences, in addition to the differences in metabolic trapping, might also be caused in part by differences in transport kinetics between GLC and FDG. We therefore used double-label quantitative autoradiography to compare transport kinetics of FDG and GLC in normal rats and in rats experiencing kainic acid-induced seizures.

METHODS

Six normal rats and four rats that had been given intraperitoneal injections of 10 mg/kg of kainic acid were anesthetized lightly with halothane and femoral arterial and venous catheters were placed. The rats were restrained by taping them to a brick

Received Dec. 31, 1991; revision accepted Apr. 16, 1992.

For reprints contact: J.L. Lear, Division of Nuclear Medicine (A034), University of Colorado Health Sciences Center, 4200 E. 9th Ave., Denver, CO.

and allowed to recover for 2 hr. Two milliliters of saline containing a mixture of 20 μCi of ^{14}C-6-GLC (American Radiolabeled Chemical, specific activity of 55 mCi/mmol) and 16 mCi of ^{18}F-FDG (carrier free, specific activity greater than 100 Ci/mmol) were then administered in a 45 sec intravenous infusion to each rat. Arterial blood samples were obtained every three sec during the tracer infusions, and plasma was rapidly separated from the whole blood. The rats were killed by decapitation at the end of the infusions, and the brains were rapidly removed and cut into halves along the interhemispheric fissure.

Two additional rats were prepared as the normal rats above, but then given 20 μCi of ^{14}C-FDG instead of ^{14}C-GLC in the infusions (along with the ^{18}F-FDG). These rats were used as controls to evaluate the types and magnitudes of errors associated with the dual tracer quantitative autoradiography.

From one half of each brain, small tissue samples weighing 5 to 20 mg were dissected from the mid-frontal cortex and central hippocampus. The samples were weighed, dissolved, and mixed with liquid scintillation fluid. The ^{18}F concentration of each sample was determined using a gamma counter. One week later, after the ^{18}F had decayed to negligible levels, the ^{14}C concentration of each sample was determined using a liquid scintillation counter.

The other half of each brain was frozen in powdered dry ice and then cut into 20 micron-thick sections using a cryomicrotome. The sections were collected on cover slips, dried on a 60° hot plate, and opposed to Kodak NMC film for 4 hr. This procedure produced exposures mostly resulting from the ^{18}F. One week later, after the ^{18}F had decayed to negligible levels, the sections and calibrated ^{14}C standards were opposed to another sheet of film for 10–20 days, producing ^{14}C exposures. The films were developed using a standard x-ray film processor, generating the autoradiograms.

Using a computer-controlled, solid-state scanner (*6*), the autoradiograms were digitized into matrices of 1024 × 1024 pixels having 256 shades of gray. The digitized images were compressed into 512 × 512 matrices to reduce noise and to facilitate subsequent processing. The corresponding images from each pair of 4-hr and 10–20-day exposures were aligned to within 1 pixel of one another using a combination of manual rotation and computer translation. Using a calibration curve derived from the ^{14}C standards, the digitized transmission-unit images were then converted on a pixel-by-pixel basis into digital images reflecting effective ^{14}C concentration. In other words, digital images were produced in which the level of gray of each pixel quantitatively reflected exposure from radionuclide decay as opposed to its original optical transmission value. This process resulted in pairs of corresponding digital images, each member of which reflected predominately ^{18}F or ^{14}C exposure, but each having units of effective ^{14}C tissue concentration (*7,8*).

The effective ^{14}C concentration-unit images were corrected for exposure cross-contamination caused by the presence of the slight amount of ^{14}C exposure in the 4-hr images (*7*) and for the presence of a small amount of residual tracer within the vasculature as opposed to tissue (*9,10*). The units of the ^{18}F-based images were then converted from effective ^{14}C concentration into ^{18}F concentration using an exposure efficiency factor (*7*). In this manner, images accurately reflecting the regional tissue concentrations of ^{18}F-FDG- and ^{14}C-GLC-derived radiolabel concentrations were produced.

For the small dissected-tissue samples and for the pixels within autoradiograph-based tracer concentration images, we generated corresponding K1 values. The method used to estimate these blood-to-brain transport rate constants (K1) was derived from the widely used two-compartment kinetic model for glucose analogs (*1,11,12*) (Fig 1).

$$dCb/dt = K1 \times Cp - k2 \times Cb, \qquad \text{Eq. 1}$$

where K1 = blood-to-brain transport rate constant of FDG or GLC, k2 = brain-to-blood transport rate constant of FDG or GLC, Cp = plasma concentration of FDG or GLC and Cb = brain concentration of FDG or GLC. In order to compute K1 from a single experimental duration, we assumed that:

$$k2 \approx 1.5 \times K1, \qquad \text{Eq. 2}$$

so that Equation 1 could be rewritten as:

$$dCb/dt \approx K1 \times (Cp - 1.5 \times Cb). \qquad \text{Eq. 3}$$

For the small dissected-tissue samples, the tracer concentration values were converted into K1 values by numerically integrating Equation 3 using the measured Cp values. The transport rate constant values (units of min^{-1} ml/g) were then compared between the GLC and FDG.

Similarly, for the autoradiograms, the tracer concentration images were converted into K1 images on a pixel-by-pixel basis by applying Equation 3 and the Cp measurements. FDG values were then compared to GLC values using region of interest (ROI) analysis, pixel-by-pixel subtraction and all-pixel-plotting.

In addition, the effects that the observed variations in K1 (FDG)/K1 (GLC) would have on FDG-based metabolic rates were evaluated. Computer simulations were used to generate two sets of LCMRglc images, one in which a fixed K1 (FDG)/K1 (GLC) ratio was used for all brain regions and the other in which the actual ratios measured in our studies were used. Images representing the pixel-by-pixel percent differences between the fixed-ratio-based and variable-ratio-based LCMRglc values were compared for the normal, kainic acid-treated and control rats.

RESULTS

Table 1 presents mean values of K1 and plasma glucose concentrations for the frontal cortex and hippocampus

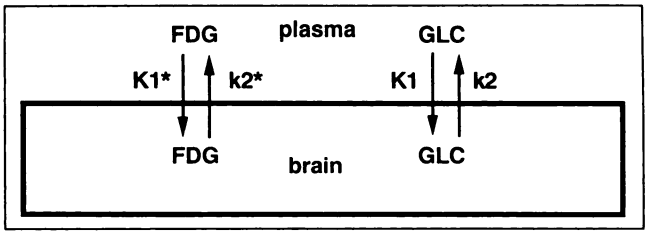

FIGURE 1. Commonly used two compartment, plasma-brain, model for glucose-analog tracer kinetics that was employed in this study. The GLC and FDG cross from the plasma to the brain via facilitated transport with rate constants of K1 and K1* respectively. They cross from the brain to the plasma with rate constants of k2 and k2* respectively. While the standard method of determining glucose metabolism using FDG assumes that the values of K1 versus K1* and of k2 versus k2* differ from each other, it requires that a fixed ratio of FDG constants divided by GLC constants applies globally. Note: metabolic rate constants are not shown because negligible metabolism occurs in the brief experiments.

TABLE 1
Mean Values of K1 and Plasma Glucose Concentrations for Frontal Cortex and Hippocampus in Dissected Tissue Samples

	FDG	GLC
Normal (9.1)		
Cortex	0.32 ± 0.05	0.31 ± 0.07
Hippocampus	0.24 ± 0.04	0.27 ± 0.06
Kainic acid-treated (17.5)		
Cortex	0.23 ± 0.04	0.25 ± 0.05
Hippocampus	0.20 ± 0.03	0.23 ± 0.03

Units: K1 = min^{-1} ml/g ± s.d. The mean value of plasma glucose concentration (mmol/liter) measured just prior to the beginning of the infusions is in parentheses. FDG values were not shown to be significantly different from corresponding GLC values in the normal or kainic acid-treated rats ($p > 0.1$).

derived from the dissected tissue samples. In the normal animals, both cortical and hippocampal FDG-based values were not significantly different from the corresponding GLC-based values ($p > 0.1$). Kainic acid-treatment caused both the FDG and GLC rate constants to drop significantly ($p < 0.05$) from baseline values, presumably a result of the large increase in plasma glucose concentration (9.1 mmol/liter control versus 17.5 stimulated). However, as in the normal animals, no large-region differences between FDG and GLC transport rate constants were demonstrated for either the hippocampus or cortex.

Data from the autoradiograms were more complex. Overall, the K1 images from FDG were similar to those from the GLC in the normal animals (Fig. 2) and kainic acid-treated animals (Fig. 3), not unexpected given the results from the tissue samples.

However, detailed examination of the quantitative images revealed different K1 patterns for FDG versus GLC in some structures, particularly the hippocampus. For example, in all six of the normal rats, ROI analysis showed that the stratum moleculare to stratum pyramidale ratio for the FDG was greater than that for the GLC, averaging 1.2 versus 1.0. The kainic acid-treatment caused these ratios to be reversed with respect to rank-order in all four rats, averaging 0.9 and 1.2 respectively, values significantly different from each other ($p < 0.02$) and from those of the normal rats ($p < 0.02$).

Such pattern differences were not observed in the control ^{14}C-FDG-^{18}F-FDG rats (Fig. 4), and therefore did not result from errors in the autoradiographic processing. In other words, real differences were found in some structures between K1 values for FDG and GLC, both in the normal and kainic-acid treated rats.

These differences in K1 patterns between FDG and GLC also were reflected in the data from the all-pixel-plots (Fig. 5). Data from the FDG-GLC comparisons showed more spread from the lines-of-identity than did the control (^{14}C-FDG-^{18}F-FDG) data, again illustrating that FDG transport was not directly correlated to GLC transport for all structures.

The simulation studies showed that these previously unappreciated regional variations in the ratio of K1 (FDG)/K1 (GLC) could cause regional variations in the "lumped constant". These variations in the "lumped constant" in turn would cause related errors in LCMRglc measurements in experiments for which a fixed "lumped constant" was assumed to apply to the entire brain (Figs. 2–4). However, the magnitude of the errors in LCMRglc was only about half that of the variations in the K1 ratio. In other words, errors in LCMRglc measurements would not be as great as the uncorrected variations in the K1 ratios that caused the errors.

DISCUSSION

Before discussing the results of our studies, it is important to consider the model and methods that were used. We used the standard two-compartment, plasma-brain model for tracer distribution (Fig. 1), and assumed for simplicity that the rate constant for brain-to-blood transport, k2, was equal to 1.5 times the rate constant for blood-to-brain transport, K1. This assumption was based on well-established differences between the size of the glucose distribution space for the plasma and brain. While this is

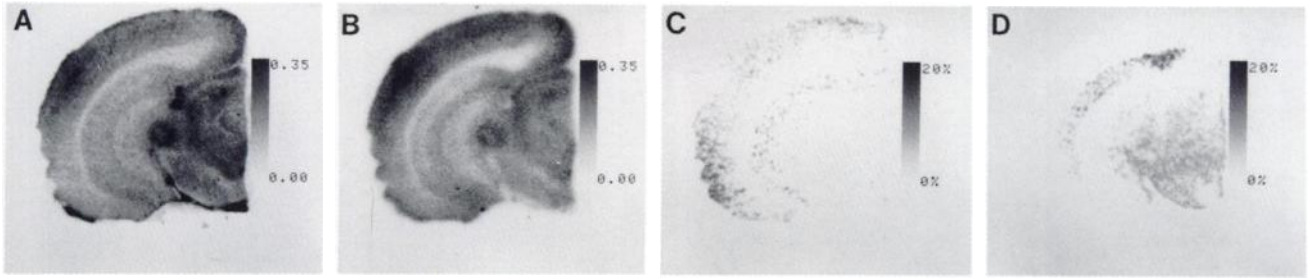

FIGURE 2. Quantitative digital images representing the transport rate constants of GLC and FDG in a normal rat. A and B are K1 images (min^{-1} ml/g) of GLC and FDG respectively. Overall, the quantitative images of K1 for FDG are similar to those for GLC. However, in some structures such as the hippocampus, the relationships between FDG and GLC transport rate constants differ from the global value. This phenomenon was observed in all of the rats in the study. C and D are simulation-based images that depict the effects that unaccounted for variations in transport would have on LCMRglc measurements. Both overestimates (C) and underestimates (D) of LCMRglc values can occur.

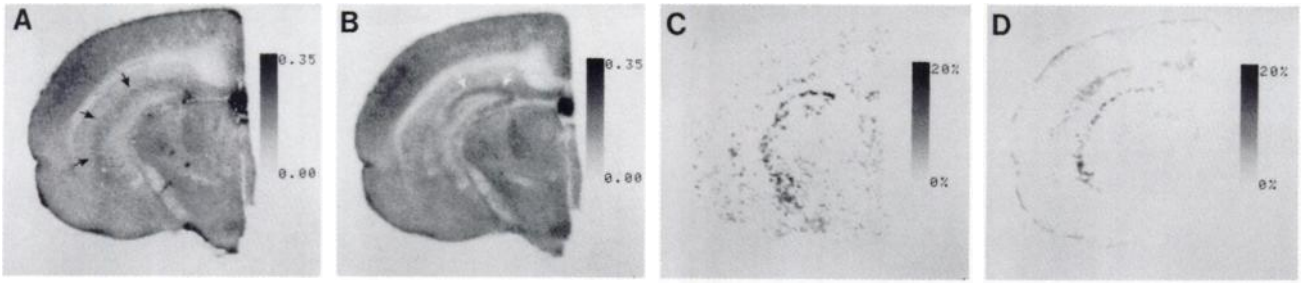

FIGURE 3. Quantitative digital images representing the transport rate constants of GLC and FDG in a kainic acid-treated rat. A and B are K1 images (min^{-1} ml/g) of GLC and FDG respectively. As in the normal animals, the quantitative images of K1 for FDG are similar to those for GLC. However, in some structures such as the hippocampus, the relationships between FDG and GLC transport rate constants differ from the global value. For example the stratum moleculare (black arrows) has relatively greater GLC transport than FDG transport, while the cell-body layer (white arrows) has relatively greater FDG transport than GLC transport. C and D are simulation-based images that depict the effects that unaccounted for variations in transport would have on LCMRglc measurements. Both overestimates (C) and underestimates (D) of LCMRglc values can occur.

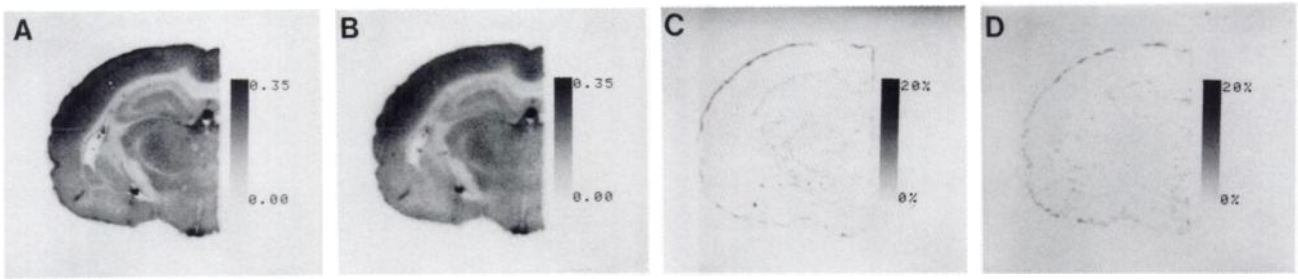

FIGURE 4. Quantitative digital images representing the transport rate constants of ^{14}C-FDG (A) and ^{18}F-FDG in a normal rat. Other than slight attenuation artifacts, the images are identical. C and D are simulation-based images corresponding to those of Figures 2 and 3. Only slight random noise is present caused by the attenuation effects and imperfect registration between the K1 images.

only an approximation, by using short experiments we reduced the effects that any errors in this assumption would have on determination of K1. At 45 sec, the duration used in these studies, the terminal ratio of the concentration of plasma tracer (FDG or GLC) to that of brain tracer was always greater than five to one. Therefore, the second term in Equation 1 (k2 × Cb) is small compared to the first term (K1 × Cp). In other words, calculated blood-to-brain rate constants are not greatly influenced by changes in assumptions regarding k2. For example, even if k2 were assumed to be zero, the calculated K1 would decrease only by about 10%.

Similarly, the brevity of the experiments eliminated the need to consider metabolism kinetics in the model. Rate constants for glucose and deoxyglucose metabolism (k3) are only about half those for transport, so that in such brief experiments, the effects of tracer metabolism on uptake patterns are insignificant (less than 5%).

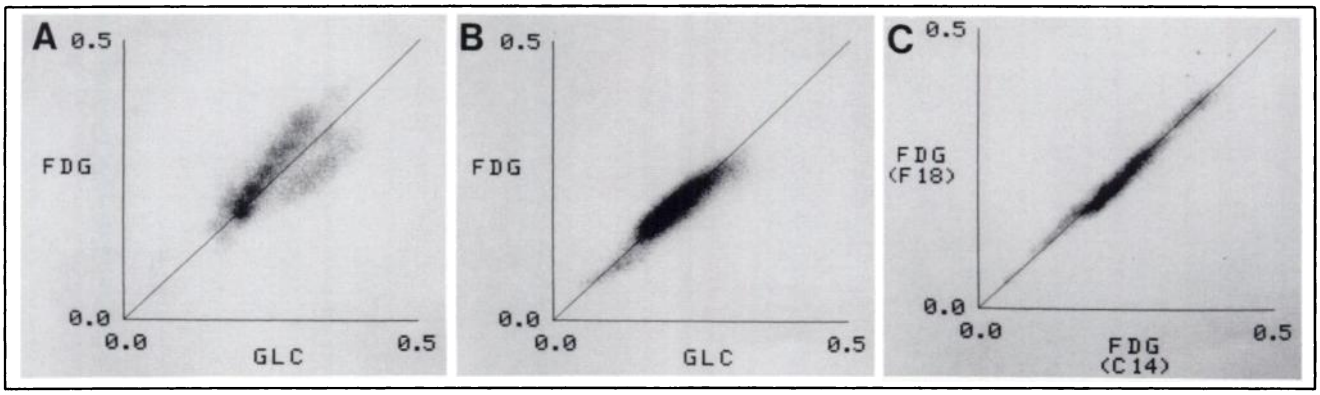

FIGURE 5. All-pixel-plots of K1 for FDG versus GLC from a normal (A) and kainic acid-treated (B) rat. Each plot represents over 1 million points obtained from four to five representative sections from each rat. A plot from a control ^{18}F-FDG-^{14}C-FDG rat (C) defines the errors associated with the dual tracer technique. If the technique were perfect, then all data would be on the line of identity. Some spread occurs, but it is less than that observed in the FDG versus GLC plots, indicating the existence of real differences between FDG and GLC.

The results of our studies can be considered on two levels of analysis: low resolution comparisons of GLC versus FDG transport based on the tissue sample data and high resolution comparisons based on the autoradiographic data. While the tissue samples were themselves small, averaging approximately 10 mg in weight, they had to be dissected from visually identifiable brain regions. This limited localization to structures on the order of several millimeters in diameter. On the other hand, the resolution of the dual tracer autoradiography is much greater, approximately 100 × 100 × 20 microns (*6,7*); moreover it offers the additional advantage of visually portraying the regional patterns of transport.

We therefore limited our use of the tissue sample data to the comparison of transport rate constant values of FDG versus GLC for only two easily identifiable regions—the frontal cortex and hippocampus. We found no significant differences for cortical values of K1 between FDG and GLC ($p > 0.1$) as well as no differences in overall hippocampal K1 values between FDG and GLC ($p > 0.1$). These results differ from those of some previous studies in which significantly greater transport rates for FDG have been reported (*13–15*). For example, data based on brain uptake index studies (*14,15*) suggest that the FDG transport rate constant is approximately 125% that of GLC at a plasma glucose concentration of 10 mmol/liter. However, the rate of uptake of FDG by the heart was found to be 94% that of GLC in a condition in which transport was limiting (*16*). The causes of the discrepancies are uncertain. A possible explanation is that our double label technique, by eliminating interanimal variability from the comparisons, yielded more valid results but it is also possible that some unappreciated error occurred in our studies. Finally, it may be there are unappreciated infusion-duration effects resulting from the serial transport of tracers from the blood to the extracellular space and then from the extracellular space to the intracellular space. If this is so, our 45 sec-based values may not be directly comparable to the 5 sec-based values (*14,15*) or to the multi-minute-based values (*16*). Further experiments may be needed to resolve these issues.

We found that the K1 values for both FDG and GLC decreased by an average of 22% between the normal and stimulated conditions in response to a rise in the mean plasma glucose concentration from a value of 9.1 mmol per liter to a value of 17.5 mmol per liter. This observed change agrees well with values from studies measuring tracer competition, in which 20% decreases in both GLC and FDG transport rate constants were reported as the glucose concentration in the infusions was increased from 10 to 20 mmol per liter (*14,15*).

Irrespective of the findings regarding the absolute values of K1 for GLC and FDG, it is important to note that the tissue sample data did not show any regional variations in the ratio of K1(FDG) to K1(GLC). In other words, the tissue sample results are entirely consistent with the standard two-compartment transport model. They therefore also support the use of a single lumped constant-value between different regions.

However, the higher resolution autoradiographic data point to a different conclusion regarding the limits of the standard transport model: that while the model applies to most brain regions, it is inaccurate in certain structures. It has been generally assumed that, although FDG and GLC have different overall kinetics, the relationships between their rates of transport and their rates of metabolism are fixed throughout the brain. However, we found that while this assumption is valid for most parts of the brain, some structures such as the hippocampus have different patterns of FDG transport compared to GLC transport. Kainic acid treatment changes the overall values of transport rate constants in these regions, but differences between FDG and GLC rate constant patterns persist. These differences are unlikely to result from some error in the autoradiography or image analysis since they were not observed in the control FDG-FDG studies.

The observed differences between the behavior of FDG and GLC cannot be accounted for using the standard two-compartment, plasma-brain model for FDG transport; some other mechanism must apply at least in the regions that have discordant K1 patterns of FDG versus GLC. One possibility is that another significant compartment exists with respect to determining net FDG versus GLC blood-to-brain transport (Fig. 6). Regional variations in the size of this hypothetical compartment could account for our observations. Another possibility is that particular brain regions may contain different populations of transporters with different affinities for FDG and GLC (Fig. 7). Depending upon the regional mixtures of the transporters, the relative rates of FDG versus GLC transport could vary.

How do these observations impact upon the use of FDG to quantify LCMRglc? Regional variations in the ratio of FDG versus GLC transport rate constants, unless exactly balanced by regional variations in the metabolic rate constants, will cause regional variations in size of the relative

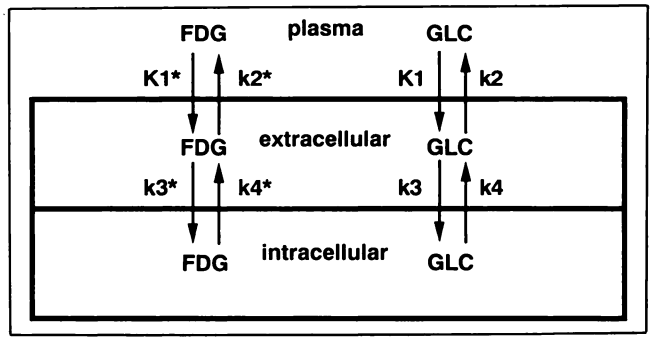

FIGURE 6. The observed differences in apparent K1/K1* ratios for certain structures could reflect the presence of more than one significant brain compartment, e.g., extracellular and intracellular compartments, with respect to substrate transport. Our findings could be explained by regional variations in the relative sizes of the two compartments.

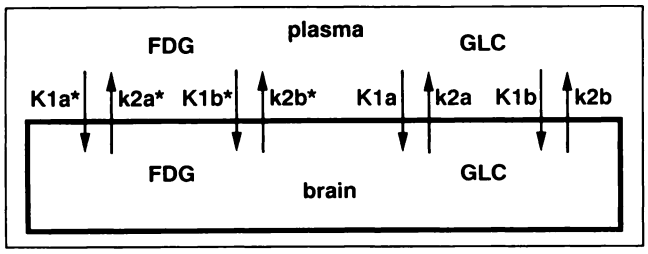

FIGURE 7. The observed differences in apparent K1/K1* ratios for certain structures could reflect the presence of different populations of transporters with different relative affinities for glucose and deoxyglucose. Our findings could be explained by regional variations in the relative densities of the different transporters.

distribution spaces of FDG and GLC. These regional variations of distribution space-size in turn will cause regional variations in the FDG "lumped constant". Therefore, if a single "lumped constant" is used for the entire brain, errors in LCMRglc determination will occur in those structures whose FDG versus GLC K1 ratios differ from mean values. However, the magnitude of these errors will be only about half as great as the unaccounted for variations in the transport rate constants in most conditions since metabolic rate constants more influence the lumped constant than do transport rate constants.

While our results do point to a limitation of the fixed lumped constant-FDG model, they are not actually inconsistent with other studies that have indicated regional stability of the "lumped constant". Such studies have been performed with single tracer techniques, or dual-tracer tissue-sampling techniques, and lacked the spatial resolution of the present study. Thus, we do not suggest that our data pose a significant problem to the practical use of the FDG method in situations with limited resolution, such as PET scanning or even most animal tissue-sampling or autoradiographic studies. Rather, we feel that the results of this study indicate a pathway for further exploration of the complicated issue of regional differences in cerebral substrate transport and metabolism.

ACKNOWLEDGMENTS

Supported by a Scholar Grant of the Radiological Society of North America (to Dr. Lear), by NIH grants NS-26657, NS-15654, and MH-037916 and DOE contract DE-AC03-76-SF00012. The authors gratefully acknowledge the efforts of Mr. Wrother Meredith, whose technical expertise made collection of these data possible. The authors also gratefully acknowledge the support and encouragement of Dr. Michael Phelps, the technical support of Dr. Jorge Barrio and the Chemistry Section and Dr. N. Satymurthy and the Cyclotron Section of the UCLA Division of Nuclear Medicine and Biophysics, who provided the ^{18}F-FDG for these experiments.

REFERENCES

1. Sokoloff L, Reivich M, Kennedy C, Des Rosiers H, Patlak C, Pettigrew K, et al. The [^{14}C]deoxyglucose method for the measurement of local cerebral glucose utilization: theory, procedure, and normal values in the conscious and anesthetized albino rat. *J Neurochem* 1977;28:897–916.
2. Lear J, Ackermann R. Comparison of cerebral glucose metabolic rates measured with fluorodeoxyglucose and glucose labeled in the 1, 2, 3–4, and 6 positions using quantitative double label autoradiography. *J Cereb Blood Flow Metab* 1988;8:575–585.
3. Duncan G, Pilgrim C, Stumpf W, McCown T, Breese G, Mueller R. High resolution autoradiographic determination of the topographic distribution of radioactivity of the hippocampal formation after injection of [1-^{14}C] glucose or 2-deoxy[^{14}C] glucose. *Neuroscience* 1986;17:99–106.
4. Ackerman R, Lear J. Glycolysis-induced discordance between cerebral glucose metabolic rates measured with fluorodeoxyglucose and glucose. *J Cereb Blood Flow Metab* 1989;9:774–785.
5. Lear J, Kasliwal R. Autoradiographic measurement of cerebral lactate transport in normal and activated conditions. *J Cereb Blood Flow Metab* 1991;11:576–580.
6. Lear J, Plotnick J, Rumley S. Digital autoradiography: design, development and performance of a solid state image analyzer. *J Nucl Med* 1987;28:218–222.
7. Lear J, Ackermann R, Kameyama M, Carson R, Phelps M. Simultaneous multiple radionuclide autoradiography in evaluation of cerebral function. *J Cereb Blood Flow Metab* 1984;4:264–269.
8. Lear J. Multiple radionuclide autoradiography: considerations in optimizing precision and accuracy. *J Cereb Blood Flow Metab* 1988;8:443–448.
9. Gjedde A, Diemer N. Double tracer study of the fine regional blood-brain glucose transfer in the rat by computer-assisted autoradiography. *J Cereb Blood Flow Metab* 1985;5:282–289.
10. Lear J, Kasliwal R, Feyerabend A. Mapping regional cerebral vascular transit times by simultaneous determination of local cerebral blood flow and local cerebral blood volume. *Metabolic Brain Dis* 1990;5:155–165.
11. Gjedde A. Rapid steady-state analysis of blood-brain glucose transfer in rat. *Acta Physiol Scand* 1980;108:331–339.
12. Hawkins R, Mans A, Davis D, Hibbard L, Lu D. Glucose availability to individual cerebral structures is correlated to glucose metabolism. *J Neurochem* 1983;40:1013–1018.
13. Fuglsang A, Lomholt M, Gjedde A. Blood-brain transfer of glucose and glucose analogs in newborn rats. *J Neurochem* 1986;46:1417–1428.
14. Crane P, Pardridge W, Braun L, Oldendorf W. Kinetics of transport and phosphorylation of 2-fluoro-2-deoxy-D-glucose in rat brain. *J Neurochem* 1983;40:160–167.
15. Pardridge W, Oldendorf W. Kinetics of blood-brain barrier transport of hexoses. *Biochim Biophys Acta* 1975;382:377–392.
16. Ng C, Holden J, DeGrado T, Raffel D, Kornguth M, Gatley S. Sensitivity of myocardial fluorodeoxyglucose lumped constant to insulin. *Am J Physiol* 1991;260:H593–H603.